THE JOURNAL OF PHYSICAL CHEMISTRY C

Article

pubs.acs.org/JPCC

Hydrogen Evolution from Metal–Surface Hydroxyl Interaction

Yuichi Fujimori, William E. Kaden, Matthew A. Brown,† Beatriz Roldan Cuenya,‡ Martin Sterrer,* and Hans-Joachim Freund

Department of Chemical Physics, Fritz-Haber-Institut der Max-Planck-Gesellschaft, Faradayweg 4-6, 14195 Berlin, Germany

Supporting Information

ABSTRACT: The redox interaction between hydroxyl groups on oxide surfaces and metal atoms and clusters deposited thereon, according to which metals get oxidized and hydrogen released, is an effective route to tune both the morphological (particle size and shape) and electronic (oxidation state) properties of oxide-supported metals. While the oxidation state of the metals can straightforwardly be probed by X-ray based methods (e.g., XPS), hydrogen is much more difficult to capture, in particular in highly reactive systems where the redox interaction takes place directly during the nucleation of the metals at room temperature. In the present study, the interaction of Pd with a hydroxylated MgO(001) surface was studied using a combination of vibrational spectroscopy, electronic structure studies including Auger parameter analysis, and thermal desorption experiments. The results provide clear experimental evidence for the redox nature of the interaction by showing a direct correlation between metal oxidation and hydrogen evolution at slightly elevated temperature (390 K). Moreover, a second hydrogen evolution pathway opens up at 500 K, which involves hydroxyl groups on the MgO support and carbon monoxide adsorbed on the Pd particles (water–gas shift reaction).

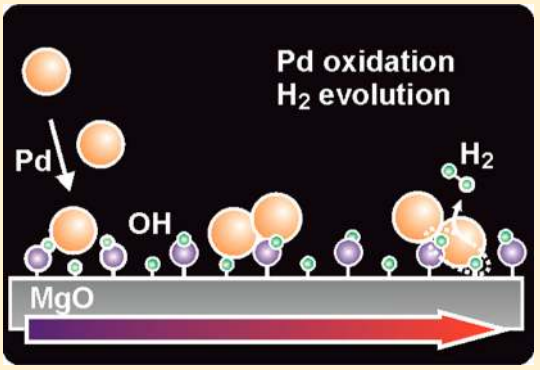

1. INTRODUCTION

Of the many barriers standing between fundamental scientific breakthroughs and their practical application to the continually growing field of nanotechnology, the robust stability of strategically designed nanostructures at dissimilar interfaces remains one of the most important to overcome. Specifically, the interactions between metals and metal-oxides are of great importance to a number of applications, ranging from heterogeneous catalysis to coating technologies relevant in the manufacture of microelectronic devices, functionalized sensors, and corrosion inhibitors, to name a few. For systems involving late-transition and noble metals adsorbed on clean metal-oxide surfaces, thermodynamics and kinetics often oppose the formation of environmentally and thermally stable metal/metal-oxide interfaces (for example, layer-by-layer metal growth in thin-film technology or maintaining high metal dispersion in catalysts).[1]

To help increase the usable range of such metastable systems, one must find ways to increase the adhesion energy between the metals and the metal-oxides, which can be accomplished via modification of the oxides' interfacial properties, such as defect concentration, surface termination, or functionalization. While much is already known about the role of defects,[2,3] there have not been many surface-science studies aimed at investigating the latter effects. Of those, one of the most obvious functional groups to explore are hydroxyls, which are often omnipresent in realistic conditions but nearly absent following ultrahigh vacuum (UHV)-based sample preparations. When exploring the role of such groups on the growth of metals over alumina supports, others noted evidence of enhanced interactions between the supported metals and the hydroxylated metal-oxide surfaces.[4−6] Based predominantly on results from X-ray photoemission spectroscopy (XPS) studies, which were used to monitor the chemical-states of the surface oxygen and supported metal species, the following redox reaction between interfacial hydroxyl groups and metals was proposed:

$$\{M^{n+} - OH^{-}\} + Me^{0} \rightarrow \{M^{n+} - O^{2-}\}Me^{+} + H(ad) \quad (1)$$

where M is a metal atom within the oxide support and Me is an atom within the supported metal particle.[4] In this scenario, the increased interaction strength of the metal with the hydroxylated oxide surface arises from enhanced ionic contributions to the metal–substrate bonding and the formation of partially oxidized metal species. A central limitation of the aforementioned studies is that the fate of hydrogen, which may either (i) remain adsorbed on the surface, as suggested in eq 1, (ii) be trapped in the deposited metal particles, as suggested by computational work,[7,8] or (iii) desorb as H_2,[5,9] cannot be directly probed and has, therefore, remained elusive in previous surface-science works.

Detection of hydrogen in/on supported metal particles is a nontrivial task. Its presence may be inferred using structural and electronic properties extracted from X-ray absorption studies

Received: May 12, 2014
Revised: July 8, 2014
Published: July 9, 2014

   dx.doi.org/10.1021/jp504655e | J. Phys. Chem. C 2014, 118, 17717–17723

and computationally derived cluster geometries,[7,10] or, using a more direct approach, one can depth-profile the abundance of H atoms within a sample using nuclear reaction analysis.[11] By contrast, probing the evolution of molecular hydrogen using mass-spectroscopic techniques during temperature-programmed desorption (TPD) experiments is relatively straightforward and provides information complementary to the alternative approaches when investigating reactions between surface hydroxyls and supported metals. For the present study, we have applied TPD in combination with infrared reflection absorption spectroscopy (IRAS), XPS, and X-ray excited Auger electron spectroscopy (XE-AES) to probe the interaction and reactivity of Pd with hydroxyls on a MgO(001) model surface. Using this approach, our specific aim is to more directly evaluate the redox process described in eq 1 by correlating the thermal evolution of molecular hydrogen as an indicator for the reactivity of the system, with changes to the electronic structure of deposited Pd.

2. EXPERIMENTAL DETAILS

The experiments were carried out in a UHV system comprising a preparation chamber and an elevated pressure cell. The preparation chamber has standard tools for single-crystal cleaning and oxide thin-film preparation installed and is equipped with a low energy electron diffraction (LEED) apparatus, a quadrupole mass spectrometer for TPD experiments, and a dual (Mg/Al) anode X-ray source combined with a hemispherical electron analyzer (Specs Phoibos 150, E_{kin} range: 0−3500 eV) for XPS. The UHV-elevated pressure cell is used for gas dosing up to atmospheric pressures and has attached an Fourier transform infrared (FTIR) spectrometer and an external MCT detector for IRAS measurements.

Well-ordered MgO(001) thin films of nominally 30 monolayer (ML) thickness were grown on a clean Ag(001) substrate by reactive deposition of Mg in an oxygen atmosphere (1×10^{-6} mbar) while maintaining a sample temperature of 570 K. The surface of the MgO(001) thin films was hydroxylated in the UHV-elevated pressure cell in a D_2O atmosphere of 0.05 mbar. Care was taken to avoid contamination of the MgO surface during the elevated pressure D_2O exposure, and the procedure has been optimized until no carbon contamination could be seen in XPS after hydroxylation. Pd was deposited on either clean MgO(001) or hydroxylated MgO at room temperature by evaporation from an electron beam evaporation source. The amount of deposited Pd was calibrated with a quartz microbalance, and the Pd coverage is given in ML, with 1 ML corresponding to $\sim 1.5 \times 10^{15}$ Pd atoms·cm^{-2}. For the experiments described in this study, Pd−MgO samples with two different Pd coverages, 0.16 and 0.4 ML, were prepared. Direct information about the average Pd particle size on these samples, for example, from scanning tunneling microscopy investigations, is not available. However, based on previous studies,[12−14] an average Pd particle diameter of 2 nm for 0.16 ML Pd and 3 nm for 0.4 ML Pd is expected for well-annealed samples. Experimental results are presented for two different sample preparations. In the first set of experiments (sections 3.1 and 3.2), Pd was deposited at room temperature onto a hydroxylated MgO surface and the properties and reactivity of the freshly prepared sample as well as changes associated with subsequent heating of this sample up to 700 K were studied. In the second set of experiments (section 3.3), Pd was first deposited onto a clean MgO(001) surface at room temperature and the sample was then heated to 700 K to allow the deposited Pd to form well-faceted particles. This sample was subsequently exposed to 0.05 mbar D_2O at room temperature. Accumulation of residual CO on the Pd particles during and after Pd deposition and during the exposure to D_2O could not be completely avoided. The amount of CO adsorbed from the residual gas background has not been controlled. However, comparison of IRAS spectra of the CO stretching region from the various samples (including samples where CO was deliberately dosed to the Pd particles) suggests that the CO coverage resulting from background adsorption is slightly less than the corresponding saturation coverage. The contribution of CO adsorbed on Pd on the reactivity of the samples will be described in detail in section 3.3.

Infrared spectra were recorded using a Bruker IFS66-V FTIR spectrometer with the resolution set to 4 cm^{-1}. Typcially, 1000 scans were averaged for one spectrum. The IRAS spectrum of a clean MgO surface was used for background correction. The heating rate during TPD measurements was 1 K/s. XPS data were acquired at an electron takeoff angle of 60° relative to the surface normal and with a pass energy of 20 eV. Pd $L_3M_{45}M_{45}$ X-ray excited Auger spectra were taken with the XPS setup using the high-energy Bremsstrahlung background accompanying the characteristic 1486.7 eV emission line of the Al Kα X-ray source for excitation of the Pd 2p core level. While the intensity of the Bremsstrahlung background is small, a reasonable Auger signal can be obtained because of the low noise level in the kinetic energy range of interest, which is equivalent to the negative binding energy region of the spectrum.

3. RESULTS AND DISCUSSION

3.1. Hydrogen Evolution from Direct Metal−OD Redox Interaction. For the experiments described below, a hydroxylated MgO model support (MgO_{hydr}) was obtained by exposing a well-ordered MgO(001)/Ag(001) thin film to 0.05 mbar water (D_2O) vapor in a dedicated UHV-elevated pressure cell. The presence of hydroxyls is confirmed by the appearance of a high binding energy (E_B) shoulder in the O 1s XP spectrum (spectrum (1) in Figure 1a) and characteristic OD vibrational bands around 2750 cm^{-1} in IRAS (spectrum (1) in Figure 1b).[15] The latter are attributed to isolated and H-bond acceptor hydroxyl groups located at various low-coordination sites on the MgO surface.[16] The coverage of hydroxyl groups for this sample has been determined to be 0.7 ± 0.1 ML (where 1 ML OD corresponds to one dissociated water molecule per surface Mg−O unit) based on the quantification method described in ref 17. (see the Supporting Information for further details about the quantification of the hydroxyl coverage.)

Starting with the vibrational data, we note that deposition of 0.1 ML Pd at room temperature (RT) gives rise to a significant reduction of the OD-IRAS signal intensity from MgO_{hydr} (spectrum (2) in Figure 1b). When depositing larger concentrations of Pd, we note continued depletion of the OD signal, such that the signal can no longer be distinguished from the background after dosing 0.4 ML Pd (spectrum (3) in Figure 1b). This observation, which is qualitatively similar to results of a previous study investigating the interaction of manganese carbonyl complexes with hydroxyls on partially dehydroxylated MgO powder,[18] points to a strong interaction between Pd and hydroxyls and identifies the latter as preferred metal nucleation sites on the MgO_{hydr} surface.

In contrast to the observed depletion of the OD-IRAS signal, the corresponding O 1s XP spectrum taken from the 0.4 ML

dx.doi.org/10.1021/jp504655e | J. Phys. Chem. C 2014, 118, 17717−17723

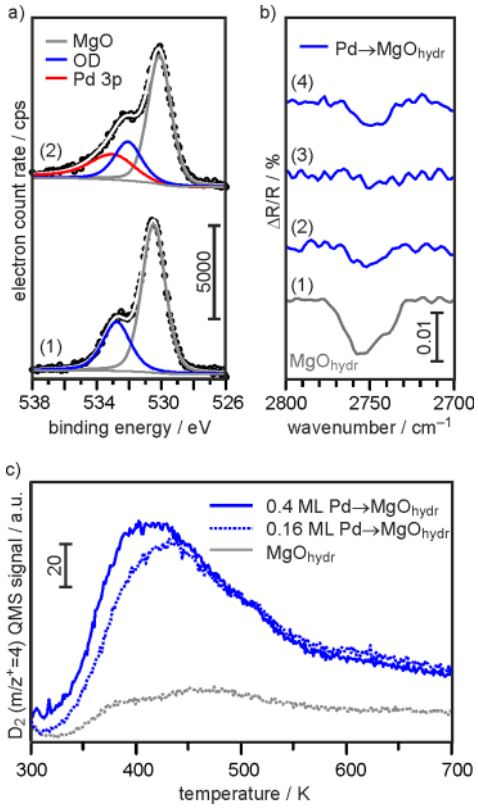

Figure 1. (a) O 1s XP spectra recorded from hydroxylated MgO before (1) and after (2) depositing 0.4 ML Pd at room temperature (black circles, data points; solid lines, results of peak fitting; see legend for assignment of individual contributions). (b) OD IRA-spectra recorded from hydroxylated MgO (1), after deposition of 0.1 ML (2) and 0.4 ML (3) Pd at room temperature, and after subsequent heating to 373 K (4). (c) TPD spectra tracking the $m/z^+ = 4$ (D_2) evolution from hydroxylated MgO (gray) and hydroxylated MgO with 0.4 ML Pd (blue, solid line) and 0.16 ML Pd (blue, dotted line) deposited at RT.

Pd−MgO_{hydr} sample (spectrum (2) in Figure 1a) continues to exhibit a clear shoulder related to hydroxyls. In fact, deconvolution of the O 1s region into its individual signal components, which is somewhat complicated by the necessary inclusion of Pd $3p_{3/2}$ contributions, reveals that the hydroxyl signal intensity is only reduced by ∼20% relative to the uncovered MgO_{hydr} sample. Since the main oxide O 1s signal experiences a similar reduction of intensity (∼15%), the partial loss of the hydroxyl O 1s signal is attributable to signal attenuation from the Pd overlayer and not to the consumption of hydroxyls by reaction with deposited Pd. In support of this conclusion is the observation that the OD-IRAS signal from Pd−MgO_{hydr} partially reappears after heating the sample to 373 K (spectrum (4) in Figure 1b). This behavior is suggested to reflect the thermally induced breakup of a part of the Pd−OD_{surf} complexes formed at RT. Therefore, both XPS and IRAS indicate negligible hydroxyl consumption, with little, if any, spontaneous reaction between hydroxyls and Pd occurring at RT.

To explore the reactivity between Pd and hydroxyls at elevated temperature, we tracked the evolution of D_2 from the samples during heating from room temperature to 700 K in a TPD experiment. Figure 1c compares the D_2 TPD signals from the hydroxylated MgO surface (gray trace) and from 0.4 ML Pd deposited on MgO_{hydr} at RT (blue trace, solid line). From the resultant plots, it is obvious that the presence of Pd leads to a strong enhancement of D_2 evolution from MgO_{hydr} at elevated temperature. D_2 desorption starts slightly above RT (350 K), exhibits a maximum between 390 and 450 K, and then slowly declines at higher temperatures. Since chemisorbed D_2/H_2 desorbs from supported Pd nanoparticles at lower temperatures (260 K for subsurface and 340 K for surface bound D/H; see Figure S2 in the Supporting Information),[11] we have attributed the D_2 evolving from our sample to the product of reactions between surface hydroxyls and Pd, as described by eq 1. Since D_2 should desorb from Pd particles as soon as it forms at these temperatures, we have used a simplified Redhead analysis to estimate the activation energy E_a for the Pd + OD_{surf} reaction, which we assume to be equal to the desorption energy associated with the D_2 TPD peak (∼1 eV).

The D_2 TPD data provides general information about the reactivity between Pd and OD_{surf}. However, we have neglected so far any influence of the Pd coverage and related effects due to different Pd particle size and morphology on the surface processes.[19] At this point, it must be mentioned that the Pd species formed by deposition at RT onto MgO_{hydr} are subjected to thermally induced rearrangement and sintering processes during the TPD run (see section 3.2), which could additionally affect the reactivity. To learn about possible effects of Pd coverage (particle size) on the Pd + OD_{surf} reactivity, we have repeated the D_2 TPD experiment with a smaller amount of Pd deposited onto MgO_{hydr} (0.16 ML Pd instead of 0.4 ML Pd; see Figure 1c, blue trace, dotted line). The similar D_2 TPD results obtained for the different Pd coverages suggest that Pd particle size has no influence on the reactivity. Moreover, this result shows that only a limited number of surface hydroxyls are involved in reactions with Pd, and that the mobility of Pd on the surface is sufficiently high to allow all reactive hydroxyls to be reached even at relatively low Pd concentrations. To estimate the number of reactive hydroxyls, we have compared the integrated time-dependent D_2 TPD peak intensity of the D_2 desorption resulting from the Pd + OD_{surf} reaction with that of D_2 desorption from chemisorbed D_2 on the surface of MgO(001)-supported Pd particles (see Figure S2 in the Supporting Information and the accompanying text, which lists all parameters and assumptions required for this estimation). From this analysis, the number of hydroxyls involved in the Pd + OD_{surf} reaction is estimated to be ∼0.05 ML OD. Unfortunately, it is not possible, based on the available data, to attribute the reactivity to a hydroxyl in a specific coordination or hydrogen bonding environment. Computational modeling could certainly help at this point to identify possible reactive hydroxyl species.

In summarizing the first part of this study, we note that our combined IRAS, XPS and TPD experiments for Pd deposited at room temperature on MgO_{hydr} have shown that hydroxyls act as preferred adsorption sites for Pd on the MgO surface. However, a reaction between Pd and OD_{surf} according to the redox mechanism (eq 1), which leads to the evolution of D_2, requires an activation barrier of ∼1 eV to be overcome. Moreover, the amount of hydroxyls involved in the redox reaction is found to be ∼0.05 ML OD, which suggests that the redox interaction between Pd and OD_{surf} is limited to a specific type of hydroxyl present on the MgO_{hydr} surface. In the following section, we report on the detailed analysis of the electronic structure of Pd deposited onto MgO_{hydr} and subsequently heated to elevated temperature, which allows us to establish a connection between

dx.doi.org/10.1021/jp504655e | J. Phys. Chem. C 2014, 118, 17717−17723

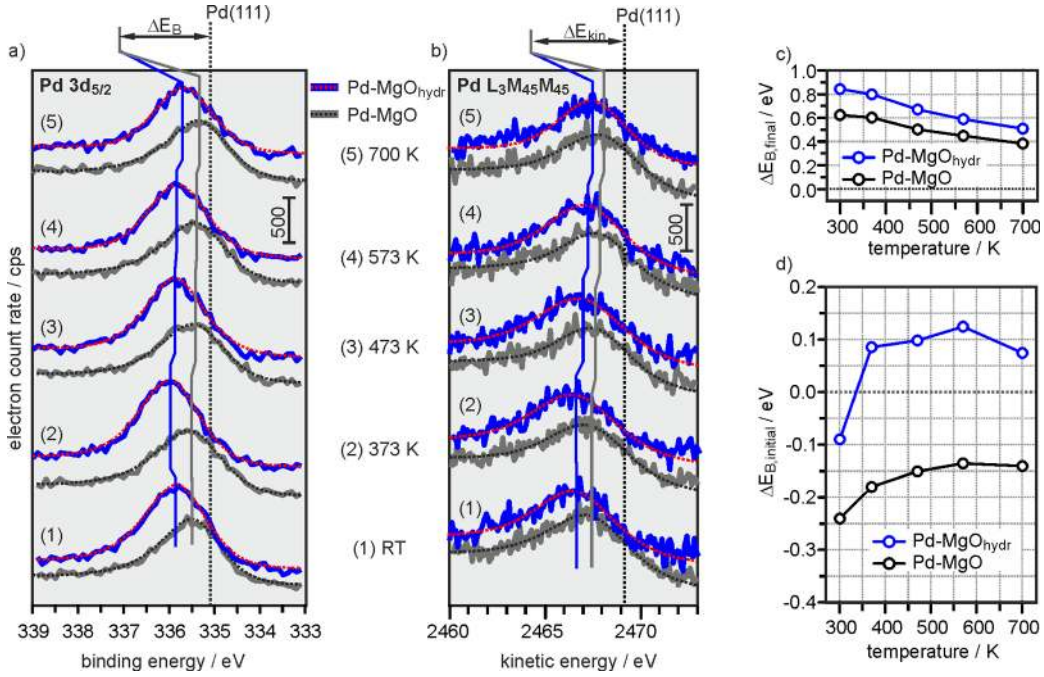

Figure 2. (Left) Pd 3d photoemission (a) and X-ray excited Pd $L_3M_{45}M_{45}$ Auger spectra (b) of 0.4 ML Pd deposited at room temperature on hydroxylated (blue) and clean MgO(001) (black). For clarity, we have chosen to show only the $3d_{5/2}$ and $^1G_4$ components of the respective data.[20,21] (Right) Temperature-dependent Pd 3d electron binding energy variations relative to Pd(111) due to changes in the final (c) and initial (d) states of the photoemission process for Pd−MgO (black) and Pd−MgO_{hydr} (blue).

Table 1. Summary of Experimentally Determined Pd 3d Electron Binding Energies (E_B) and Pd $L_3M_{45}M_{45}$ Auger Kinetic Energies (E_{kin}) and Results of the Auger Parameter Analysis for 0.4 ML Pd Deposited at RT on Unhydroxylated and Hydroxylated MgO(001) as a Function of Temperature

sample	Pd−MgO(001)/**Pd−MgO_{hydr}**				
temperature/K	300	373	473	573	700
E_B Pd $3d_{5/2}$/eV[a]	335.48/**335.85**	335.52/**335.98**	335.45/**335.87**	335.41/**335.81**	335.34/**335.68**
E_{kin} Pd $L_3M_{45}M_{45}$/eV[a]	2467.48/**2466.67**	2467.48/**2466.63**	2467.75/**2467.0**	2467.9/**2467.22**	2468.1/**2467.22**
$\Delta E_{B,3d}$/eV[b]	0.38/**0.75**	0.42/**0.88**	0.35/**0.77**	0.31/**0.71**	0.24/**0.58**
$\Delta E_{kin,LMM}$/eV[b]	−1.62/**−2.43**	−1.62/**−2.47**	−1.35/**−2.10**	−1.2/**−1.88**	−1.0/**−1.59**
$\Delta E_{B,final}$ (= $-\Delta R_{3d}$)/eV[c]	0.62/**0.84**	0.60/**0.80**	0.50/**0.67**	0.45/**0.59**	0.38/**0.51**
$\Delta E_{B,initial}$ ($-\Delta\varepsilon_{3d}$)/eV[c]	−0.24/**−0.09**	−0.18/**0.08**	−0.15/**0.10**	−0.14/**0.12**	−0.14/**0.07**

[a]Pd $3d_{5/2}$ binding energies and Pd $L_3M_{45}M_{45}$ kinetic energies were obtained from the spectral fits shown in Figure 2a and b, respectively. [b]$\Delta E_{B,3d}$ and $\Delta E_{kin,LMM}$ were calculated using measured reference values for Pd(111), 335.1 eV ($3d_{5/2}$) and 2469.1 eV ($^1G_4$). [c]Final state ($\Delta E_{B,final}$) and initial state ($\Delta E_{B,initial}$) contributions to the total Pd 3d binding energy shift were obtained through $\Delta E_{B,final} = -\Delta R_{3d} = -1/2(\Delta\beta) = -1/2[\Delta E_{B,3d} + \Delta E_{kin,LMM}]$ and $\Delta E_{B,initial} = -\Delta\varepsilon_{3d} = \Delta E_{B,3d} - \Delta E_{B,final}$.

the D_2 evolution and the surface chemistry on the Pd−MgO_{hydr} sample throughout the reaction sequence.

3.2. Correlation between D_2 Evolution and Pd Electronic Structure Changes. To reliably evaluate the effect of the interaction with hydroxyls on the nucleation and electronic properties of Pd deposited on MgO, we compare the photoemission results for the Pd−MgO_{hydr} sample with those of an analogous set of experiments performed with Pd deposited on an unhydroxylated MgO(001) surface. In Figure 2a, we show Pd $3d_{5/2}$ XPS signals from 0.4 ML Pd−MgO_{hydr} and 0.4 ML Pd−MgO(001) obtained directly after deposition of Pd at room temperature, and after subsequent heating steps up to 700 K. For both samples the resultant Pd $3d_{5/2}$ E_B's are shifted to more positive values compared to the E_B of the Pd(111) reference sample (335.1 eV, vertical dotted line in Figure 2a; see also Table 1).

Before getting into more detail about the meaning of the observed E_B shifts, we recall that for model systems consisting of small metal particles supported on insulating materials in particular, the interpretation of core-level binding energies in photoemission spectra is often complicated by the presence of both *initial-state* and *final-state* contributions.[22−24] *Initial-state* effects typically refer to variation of the *initial-state* orbital energy $\varepsilon(i)$ in the atom from which the photoelectron originates. Possible reasons for such shifts, which may occur in both positive and negative directions relative to the $\varepsilon(i)$ in a bulk reference sample are, for example, charge transfer, lattice contraction, or coordination effects (surface core-level shifts). *Final-state* E_B shifts, which are always positive, arise from a reduced *final-state* relaxation energy R (i.e., the reduced efficiency of electrons to screen the core-hole created during the photoemission process) in small metal particles compared to their bulk counterparts and the magnitude of such final-state E_B shifts is inversely proportional to the particle diameter. For the present case, it is absolutely necessary to determine the final-state contributions, since thermally induced Pd particle

dx.doi.org/10.1021/jp504655e | J. Phys. Chem. C 2014, 118, 17717−17723

size changes due to agglomeration and sintering during heating the freshly deposited Pd particles from RT to 700 K are expected to affect the measured E_B in addition to initial-state shifts caused by reaction-induced electronic structure changes.

To provide a means for experimentally deconvoluting these effects, we have made use of modified Auger parameter (β) analysis.[25,26] According to the derivations given in refs 25 and 26, ΔR, the *final-state* relaxation energy contribution, is linked to shifts in core-level E_B's determined by XPS and Auger kinetic energies (E_{kin}'s) determined by XE-AES, relative to a bulk reference sample, via:

$$\Delta R(i) = 1/2(\Delta\beta) = 1/2[\Delta E_B(i) + \Delta E_{kin}(jii)] \quad (2)$$

where *j*,*i* denote the core levels involved in the photoemission and Auger processes. The notation given in eq 2 takes into account that both transitions result in *final-states* with core-holes exclusively within the same electronic subshell (i). This choice of transitions minimizes the potential for erroneous contributions arising from estimations inherent to the derivation of $\Delta\beta$.[26,27] For determination of ΔR between the Pd particles on MgO_{hydr} or MgO, and Pd(111) single-crystal as a reference, we therefore determined both the E_B shifts of the Pd $3d_{5/2}$ core levels (Figure 2a, Table 1) and the E_{kin} shifts of the Pd $L_3M_{45}M_{45}$ Auger lines (Figure 2b, Table 1).

As ΔE_B's are defined as

$$\Delta E_B(i) = -\Delta\varepsilon(i) - \Delta R(i) \quad (3)$$

it is relatively straightforward to back out the *initial-state* orbital-energy shifts ($\Delta\varepsilon(i)$) once the ΔR's have been determined by eq 2. *Initial-state* and *final-state* contributions to the observed E_B shift are then obtained via $\Delta E_{B,initial}(i) = -\Delta\varepsilon(i)$, and $\Delta E_{B,final}(i) = -\Delta R(i)$, since, by convention, $\Delta\varepsilon$ and ΔR refer to orbital energies and $E_B(i) = -\varepsilon(i)$.

Results of the Auger parameter analysis are provided in Figure 2, where we compare changes to the Pd electronic structure of Pd−MgO_{hydr} (blue) and unhydroxylated Pd−MgO(001) (black) samples as a function of annealing temperature (see Table 1). At RT, the $3d_{5/2}$ XPS features for Pd on the hydroxylated and unhydroxylated samples (Figure 2a) appear at E_B's of ∼0.7 and ∼0.4 eV above the Pd(111) reference sample (335.1 eV). For the same samples, we note ∼2.4 and ∼1.6 eV decreases in the E_{kin}'s of the $L_3M_{45}M_{45}$ features (Figure 2b) relative to those from the bulk reference (2469.1 eV). The decomposition into $\Delta E_{B,final}$ and $\Delta E_{B,initial}$ shows that for both samples the shifts to positive E_B result predominantly from large *final-state* contributions (+0.6 eV for Pd-MgO(001) and +0.8 eV for Pd-MgO_{hydr}, Figure 2c), reflecting the inability of small, isolated Pd particles formed on the MgO_{hydr} and MgO(001) surfaces to screen *final-state* core-holes as efficiently as the bulk metal. Indeed, $\Delta E_{B,final}$ is so large that the corresponding $\Delta E_{B,initial}$ is negative for both samples (Figure 2d), suggesting that the *initial-state* orbital energies of Pd atoms in the Pd particles grown at RT on MgO_{hydr} or MgO(001) are shifted toward smaller values (closer to the Fermi energy) compared to Pd(111). Such $\Delta E_{B,initial}$ shifts are not entirely unexpected for small Pd particles on MgO surfaces and may result from a combination of (i) charge-transfer from MgO into Pd, which, according to computational studies, is expected to be small, and (ii) *initial-state* orbital energy shifts associated with the variation of the valence electronic structure of Pd atoms in reduced coordination environment (known as surface core-level shift).[24,28] (Note that without inclusion of final-state effects the E_B shifts detected with XPS in Figure 2a could have erroneously been interpreted as charge transfer from Pd to MgO.) The $E_{B,initial}$ shift being smaller for Pd on the hydroxylated sample can be taken as evidence that MgO_{hydr} is slightly more electronegative than the unhydroxylated surface. Notably, the results of the Auger parameter analysis suggest that Pd particles nucleated at RT on the MgO_{hydr} surface are not oxidized, supporting our previous conclusion that there is almost no chemical interaction between Pd and OD_{surf} at RT.

As the samples are heated, we note decreasing contributions of $\Delta E_{B,final}$ with increasing temperature in both cases (Figure 2c). This trend is readily explained by the thermally induced growth of Pd particles, which typically occurs as more energy is put into the system. That the absolute size of $\Delta E_{B,final}$ is consistently larger for Pd−MgO_{hydr} than it is for Pd−MgO(001), is consistent with the aforementioned preference for Pd adsorption at more strongly interacting hydroxyl sites, which diminishes the effects of sintering and results in the formation of smaller particles on the hydroxylated surface. Unlike $\Delta E_{B,final}$, $\Delta E_{B,initial}$ shows markedly different behavior for the two samples as a function of temperature (Figure 2d). As discussed above, at RT the initial-state Pd 3d E_B's are very close to those from bulk, but slightly shifted toward the Fermi level in both cases. As both surface core-level shift and charge-transfer effects become increasingly less significant with increasing particle size, we expect a gradual shift of $\Delta E_{B,initial}$ toward 0 with increasing annealing temperature, barring other changes to the sample, and such behavior is exactly what we observe for Pd supported on MgO(001). In contrast, $\Delta E_{B,initial}$ shifts abruptly (and permanently) to positive values after heating Pd−MgO_{hydr} to 373 K. The direction of the shift is consistent with partial oxidation of Pd particles. Moreover, comparison with the TPD data in Figure 1c shows a correlation between this shift and the onset of D_2 evolution from the Pd−MgO_{hydr} sample. The interrelation of these processes provides direct evidence of the redox reaction between Pd and hydroxyls, which results in Pd oxidation and hydrogen (deuterium) evolution.

The 0.25−0.3 eV initial-state energy difference noted between Pd on MgO and MgO_{hydr} is small compared to typical E_B differences between metallic Pd and PdO (ΔE_B = 2 eV)[20] and indicates that the extent of Pd particle oxidation on Pd−MgO_{hydr} is small. This is not surprising considering (i) the rather small amount of hydroxyls involved in the reaction (∼0.05 ML) and (ii) the fact that only the interfacial Pd atoms are being oxidized. We further note that the activation barrier for the reaction between Pd and hydroxyls on MgO is higher than that for other systems investigated previously. For example, Rh, Co, and Cu have been found to instantaneously react with hydroxyls on alumina at RT.[4−6] Differences in reactivity are not unexpected since the interaction strength between metals and hydroxyls depends on the properties of the reactants (acidity of hydroxyl groups, oxygen affinity of metals). Concerning Pd−MgO_{hydr}, the reactivity is likely limited by the high basicity of hydroxyls on MgO since the oxygen affinity of Pd should be comparable with that for Rh. For the purpose of this study, the higher activation barrier is beneficial, because this allowed, in contrast to previous studies investigating more reactive model systems,[4−6] the direct monitoring of evolving hydrogen (D_2), in addition to Pd electronic structure changes, during the interaction between Pd and hydroxyls on MgO at elevated temperature.

3.3. Involvement of Hydroxyls in Water−Gas Shift-Type (WGS) Reactions. The involvement of support

dx.doi.org/10.1021/jp504655e | J. Phys. Chem. C 2014, 118, 17717−17723

hydroxyls in the oxidation of transition-metal atoms was first highlighted in studies that dealt with the interaction of metal−carbonyl complexes with oxide surfaces.[29] Under such conditions, hydrogen desorption occurs at 470−570 K during the thermal decomposition of the carbonyls,[30] and is accompanied by the concomitant desorption of CO_2, which provides an indication that such H_2 originates from water−gas shift (WGS) reactions between the carbonyl ligands and support-bound hydroxyls.[31] Since the adventitious adsorption of residual CO could not be eliminated in our experiments, possible contributions from WGS-type reactions during the processes observed over the Pd−MgO_{hydr} samples cannot be completely excluded.

Experimental indication for such a scenario comes from Figure 3a, where we plot the simultaneously recorded D_2, CO and CO_2 TPD spectra from 0.4 ML Pd deposited on MgO_{hydr}. In addition to the previously discussed D_2 desorption from this sample with a desorption maximum at ∼410 K, a distinct desorption peak at 500 K resulting from Pd-adsorbed CO and a concomitant broad CO_2 desorption signal peaking at 500 K, which overlaps with the high temperature tail of the D_2 evolution, is detected. This result suggests that a high temperature WGS pathway (Figure 3c, right) may also be present in addition to the direct Pd−OD_{surf} reaction at around 410 K (Figure 3c, left).

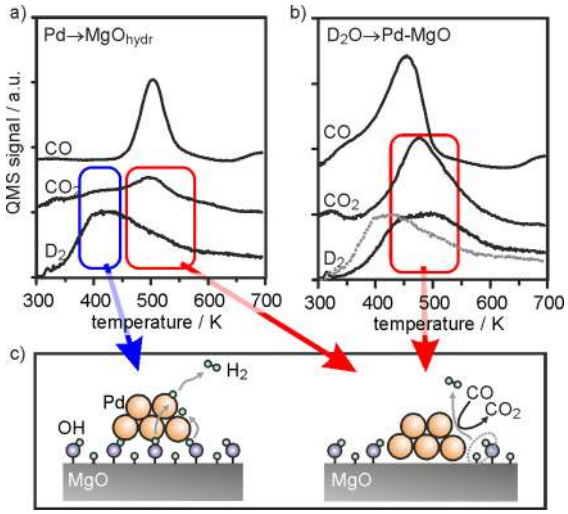

Figure 3. D_2, CO_2, and CO-TPD traces from (a) 0.4 ML Pd deposited on MgO_{hydr} (Pd → MgO_{hydr}) and (b) from a hydroxylated (0.05 mbar D_2O) 0.4 ML Pd−MgO sample (D_2O → Pd−MgO). For comparison, the D_2 TPD result from Pd → MgO_{hydr} is shown in (b) as gray trace. (c) Model depicting the various processes (left, direct redox process; right, water−gas-shift) resulting in the evolution of D_2(H_2).

To add experimental support to this hypothesis, a sample was prepared where the sequence of Pd deposition and hydroxylation was reversed; that is, Pd was first deposited onto a clean MgO(001) surface and subsequently annealed to produce well-ordered Pd particles, and this sample was then hydroxylated via exposure to 0.05 mbar D_2O at RT (D_2O → Pd−MgO). Due to the presence of traces of CO during the elevated pressure D_2O dosing, the post-hydroxylation of the Pd−MgO sample creates a situation where well-faceted Pd particles are covered by CO (see CO TPD trace in Figure 3b) and surrounded by support hydroxyl groups. Since the direct Pd−OD_{surf} redox interaction is expected to be strongly suppressed for this sample preparation, this will allow us to study the involvement of the peripheral hydroxyl groups and CO in D_2 evolution via WGS-type interactions separately.

The corresponding D_2-TPD result (Figure 3b) shows that both the onset of D_2 evolution and its maximum are shifted to higher temperature relative to the D_2 desorption trace from Pd−MgO_{hydr} (compare black and gray D_2 desorption traces in Figure 3b). The D_2 desorption maximum at 450−500 K lines up with the CO_2 desorption (Figure 3b), providing further evidence to support the existence of a WGS-type interaction between the hydroxyls on the MgO_{hydr} surface and CO adsorbed on the Pd particles. Additionally, as the contribution of D_2 desorbing at low temperature (<400 K) from this sample is considerably reduced, this result also supports our assignment of the low-temperature D_2 desorption to the direct redox reaction between Pd and OD, which is less likely in this case because of the decreased probability of direct Pd−OD_{surf} interactions.

4. SUMMARY

In summary, by combining results from vibrational spectroscopy, electronic structure studies, and thermal desorption experiments, the interaction of Pd with hydroxyl groups on a MgO(001) surface has been shown to proceed in three steps: (i) Hydroxyl groups act as the preferred adsorption sites for gas-phase deposited Pd atoms; (ii) a small percentage of the Pd-hydroxyl adsorption complexes react to yield oxidized Pd and hydrogen according to the direct redox process; and (iii) a second hydrogen production pathway opens up at elevated temperature, which involves hydroxyls at the periphery of the metal particles and Pd-adsorbed CO (water−gas shift). Consistent with the conclusions of previous studies investigating different metal/metal-oxide systems,[4−6,32−34] the processes outlined above facilitate increased particle dispersion via stronger metal−support interactions between the Pd adatoms and the hydroxylated MgO surface. Moreover, the direct correlation noted between the temperature dependence for Pd-oxidation and D_2 evolution during TPD from the hydroxylated samples helps elaborate upon, and provide a more direct level of proof for, the previously proposed redox reaction's role in governing this effect.

■ ASSOCIATED CONTENT

Ⓢ Supporting Information

Description of the quantification procedures for determination of the hydroxyl coverage and the concentration of reacted hydroxyls. This material is available free of charge via the Internet at http://pubs.acs.org.

■ AUTHOR INFORMATION

Corresponding Author

*E-mail: sterrer@fhi-berlin.mpg.de. Phone: +49 30 8413 4132.

Present Addresses

†M.A.B.: Department of Materials, ETH Zürich, Switzerland.

‡B.R.C.: Department of Physics, Ruhr-Universität Bochum, Germany.

Notes

The authors declare no competing financial interest.

■ ACKNOWLEDGMENTS

Y.F. acknowledges financial support from DAAD and Co. Ltd. Takata. M.A.B. and W.E.K. are grateful to the Alexander-von-

Humboldt Foundation for financial support. B.R.C is thankful to the Fritz-Haber-Institut der Max-Planck-Gesellschaft and the Cluster of Excellence RESOLV (DFG EXC-1069) for financial support.

REFERENCES

(1) Campbell, C. T. Ultrathin Metal Films and Particles on Oxide Surfaces: Structural, Electronic and Chemisorptive Properties. *Surf. Sci. Rep.* **1997**, *27*, 1−111.
(2) Sterrer, M.; Yulikov, M.; Fischbach, E.; Heyde, M.; Rust, H. P.; Pacchioni, G.; Risse, T.; Freund, H.-J. Interaction of Gold Clusters with Color Centers on MgO(001) Films. *Angew. Chem., Int. Ed.* **2006**, *45*, 2630−2632.
(3) Matthey, D.; Wang, J. G.; Wendt, S.; Matthiesen, J.; Schaub, R.; Laegsgaard, E.; Hammer, B.; Besenbacher, F. Enhanced Bonding of Gold Nanoparticles on Oxidized TiO_2(110). *Science* **2007**, *315*, 1692−1696.
(4) Libuda, J.; Frank, M.; Sandell, A.; Andersson, S.; Bruhwiler, P. A.; Bäumer, M.; Martensson, N.; Freund, H.-J. Interaction of Rhodium with Hydroxylated Alumina Model Substrates. *Surf. Sci.* **1997**, *384*, 106−119.
(5) Chambers, S. A.; Droubay, T.; Jennison, D. R.; Mattsson, T. R. Laminar Growth of Ultrathin Metal Films on Metal Oxides: Co on Hydroxylated α-Al_2O_3(0001). *Science* **2002**, *297*, 827−831.
(6) Kelber, J. A.; Niu, C. Y.; Shepherd, K.; Jennison, D. R.; Bogicevic, A. Copper Wetting of α-Al_2O_3(0001): Theory and Experiment. *Surf. Sci.* **2000**, *446*, 76−88.
(7) Vayssilov, G. N.; Gates, B. C.; Rösch, N. Oxidation of Supported Rhodium Clusters by Support Hydroxy Groups. *Angew. Chem., Int. Ed.* **2003**, *42*, 1391−1394.
(8) Hu, C. H.; Chizallet, C.; Mager-Maury, C.; Corral-Valero, M.; Sautet, P.; Toulhoat, H.; Raybaud, P. Modulation of Catalyst Particle Structure upon Support Hydroxylation: Ab-initio Insights into Pd-13 and Pt-13/γ-Al_2O_3. *J. Catal.* **2010**, *274*, 99−110.
(9) Sanz, J. F.; Hernandez, N. C. Mechanism of Cu Deposition on the α-Al_2O_3(0001) Surface. *Phys. Rev. Lett.* **2005**, *94*, 016104.
(10) Mistry, H.; Behafarid, F.; Bare, S. R.; Roldan Cuenya, B. Pressure-Dependent Effect of Hydrogen Adsorption on Structural and Electronic Properties of Pt/γ-Al_2O_3 Nanoparticles. *ChemCatChem* **2014**, *6*, 348−352.
(11) Wilde, M.; Fukutani, K.; Naschitzki, M.; Freund, H.-J. Hydrogen Absorption in Oxide-supported Palladium Nanocrystals. *Phys. Rev. B* **2008**, *77*, 113412.
(12) Xu, C.; Oh, W. S.; Liu, G.; Kim, D. Y.; Goodman, D. W. Characterization of Metal Clusters (Pd and Au) Deposited on Various Metal Oxide Surfaces (MgO and TiO_2). *J. Vac. Sci. Technol., A* **1997**, *15*, 1261−1268.
(13) Bäumer, M.; Freund, H.-J. Metal Deposits on Well-Ordered Oxide Films. *Prog. Surf. Sci.* **1999**, *61*, 127−198.
(14) Schalow, T.; Brandt, B.; Starr, D. E.; Laurin, M.; Shaikhutdinov, S. K.; Schauermann, S.; Libuda, J.; Freund, H.-J. Particle Size Dependent Adsorption and Reaction Kinetics on Reduced and Partially Oxidized Pd Nanoparticles. *Phys. Chem. Chem. Phys.* **2007**, *9*, 1347−1361.
(15) Carrasco, E.; Brown, M. A.; Sterrer, M.; Freund, H.-J.; Kwapien, K.; Sierka, M.; Sauer, J. Thickness-dependent Hydroxylation of MgO(001) Thin Films. *J. Phys. Chem. C* **2010**, *114*, 18207−18214.
(16) Chizallet, C.; Costentin, G.; Che, M.; Delbecq, F.; Sautet, P. Infrared Characterization of Hydroxyl Groups on MgO: A Periodic and Cluster Density Functional Theory Study. *J. Am. Chem. Soc.* **2007**, *129*, 6442−6452.
(17) Liu, P.; Kendelewicz, T.; Brown, G. E.; Parks, G. A. Reaction of Water with MgO(100) Surfaces. Part I: Synchrotron X-ray Photoemission Studies of Low-Defect Surfaces. *Surf. Sci.* **1998**, *412/413*, 287−314.
(18) Khabuanchalad, S.; Wittayakun, J.; Lobo-Lapidus, R. J.; Stoll, S.; Britt, R. D.; Gates, B. C. Formation of a Manganese Tricarbonyl on the MgO Surface from $Mn_2(CO)_{10}$: Characterization by Infrared, Electron Paramagnetic Resonance, and X-ray Absorption Spectroscopies. *J. Phys. Chem. C* **2010**, *114*, 17212−17221.
(19) Corral Valero, M.; Raybaud, P.; Sautet, P. Nucleation of Pd_n (n = 1−5) Clusters and Wetting of Pd Particles on γ-Al_2O_3 Surfaces: A Density Functional Theory Study. *Phys. Rev. B* **2007**, *75*, 045427.
(20) Moulder, J. F.; Stickle, W. F.; Sobol, P. E.; Bomben, K. D. *Handbook of X-ray Photoelectron Spectroscopy*; Perkin-Elmer Corporation, Eden Prairie, MN, 1992.
(21) Kleiman, G. G.; Landers, R.; de Castro, S. G. C.; de Siervo, A. High-Energy Auger Line Shapes of Pd and Rh: Experiment and Theory. *Phys. Rev. B* **1998**, *58*, 16103−16109.
(22) Citrin, P. H.; Wertheim, G. K. Photoemission from Surface-Atom Core Levels, Surface Densities of States, and Metal-Atom Clusters: A Unified Picture. *Phys. Rev. B* **1983**, *27*, 3176−3200.
(23) Richter, B.; Kuhlenbeck, H.; Freund, H.-J.; Bagus, P. S. Cluster Core-Level Binding-Energy Shifts: The Role of Lattice Strain. *Phys. Rev. Lett.* **2004**, *93*, 026805.
(24) Kaden, W. E.; Wu, T. P.; Kunkel, W. A.; Anderson, S. L. Electronic Structure Controls Reactivity of Size-Selected Pd Clusters Adsorbed on TiO_2 Surfaces. *Science* **2009**, *326*, 826−829.
(25) Wagner, C. D. Chemical-Shifts of Auger Lines, and Auger Parameter. *Faraday Discuss.* **1975**, *60*, 291−300.
(26) Hohlneicher, G.; Pulm, H.; Freund, H.-J. On the Separation of Initial and Final State Effects in Photoelectron Spectroscopy Using an Extension of the Auger-parameter Concept. *J. Electron Spectrosc. Relat. Phenom.* **1985**, *37*, 209−224.
(27) Bagus, P. S.; Wieckowski, A.; Freund, H.-J. Initial and Final State Contributions to Binding-energy Shifts Due to Lattice Strain: Validation of Auger Parameter Analyses. *Chem. Phys. Lett.* **2006**, *420*, 42−46.
(28) Kozlov, S. M.; Aleksandrov, H. A.; Goniakowski, J.; Neyman, K. M. Effect of MgO(100) Support on Structure and Properties of Pd and Pt Nanoparticles with 49−155 Atoms. *J. Chem. Phys.* **2013**, *139*, 084701.
(29) Burwell, R. L.; Brenner, A. Nature of $Mo(CO)_6$-Alumina Catalysts for Metathesis of Olefins. *J. Mol. Catal.* **1976**, *1*, 77−84.
(30) Brenner, A.; Hucul, D. A. Catalysts of Supported Iron Derived from Molecular Complexes Containing One, Two and Three Iron Atoms. *Inorg. Chem.* **1979**, *18*, 2836−2840.
(31) Smith, A. K.; Theolier, A.; Basset, J. M.; Ugo, R.; Commereuc, D.; Chauvin, Y. Hydrocarbon Formation from Metal-Carbonyl Clusters Supported on Highly Divided Oxides. *J. Am. Chem. Soc.* **1978**, *100*, 2590−2591.
(32) Brown, M. A.; Carrasco, E.; Sterrer, M.; Freund, H.-J. Enhanced Stability of Gold Clusters Supported on Hydroxylated MgO(001) Surfaces. *J. Am. Chem. Soc.* **2010**, *132*, 4064−4065.
(33) Veith, G. M.; Lupini, A. R.; Dudney, N. J. Role of pH in the Formation of Structurally Stable and Catalytically Active TiO_2-Supported Gold Catalysts. *J. Phys. Chem. C* **2009**, *113*, 269−280.
(34) Matos, J.; Ono, L. K.; Behafarid, F.; Croy, J. R.; Mostafa, S.; DeLaRiva, A. T.; Datye, A. K.; Frenkel, A. I.; Roldan Cuenya, B. In-situ Coarsening Study of Inverse Micelle-Prepared Pt Nanoparticles Supported on γ-Al_2O_3: Pretreatment and Environmental Effects. *Phys. Chem. Chem. Phys.* **2012**, *14*, 11457−11467.